Rotating black hole surrounded by self-gravitating torus in the puncture framework

Masaru Shibata

Graduate School of Arts and Sciences, University of Tokyo, Komaba, Meguro, Tokyo 153-8902, Japan
(Received 9 January 2007; revised manuscript received 11 July 2007; published 27 September 2007)

We present a formulation for computing equilibria composed of a rotating black hole and a massive self-gravitating torus in general relativity. Such a system is a plausible outcome formed after stellar core collapse of massive and supermassive stars as well as after a merger of a black hole-neutron star binary. In our formulation, the black hole is modeled in the puncture framework. The numerical solutions for equilibria are computed for rapidly rotating black holes and for a wide range of mass ratio of the black hole and torus. The equilibria obtained in this paper can be used for studying nonaxisymmetric instabilities, runaway instability, and magnetorotational instability of a self-gravitating accretion torus around a rotating black hole in numerical relativity. We also remark that the relation among the area, mass, and spin of rotating black holes are slightly modified by the torus.

DOI: 10.1103/PhysRevD.76.064035 PACS numbers: 04.25.Dm, 04.30.−w, 04.40.Dg

I. INTRODUCTION

A system composed of a rotating black hole and a self-gravitating torus is a possible outcome formed after stellar core collapse of a massive star [1], after the merger of a black hole-neutron star binary [2–4], and after the collapse of a supermassive star [5]. Because the torus is likely to be very hot due to shock heating in the formation process, the stellar-mass outcome could be a central engine of gamma-ray bursts [1,6]. It also may be a strong source of gravitational waves because the self-gravitating torus is often unstable against nonaxisymmetric deformation [7]. A class of torus is also subject to the runaway instability which has been studied in a number of articles; e.g., [8] and references cited therein. These facts motivate study for the black hole-torus system.

For the study of dynamical properties of a black hole-torus system such as stabilities against nonaxisymmetric deformation and against runaway instability, numerical simulation in general relativity is the best approach. Until quite recently, the numerical method for the long-term evolution of a system composed of a black hole and matter had not been developed in full general relativity, and hence, simulation for the black hole-torus system has not been done yet. However, numerical relativity has been significantly developed in the past few years. For example, it has already been a feasible task to perform general relativistic hydrodynamic simulations for the merger of binary neutron stars [9,10], for stellar core collapse with a realistic equation of state [11], for the collapse of supermassive stars [5,12], and for magnetorotational collapse [13], which were unsolved issues several years ago. A long-term evolution for black hole spacetime was only one remaining issue to be resolved a few years ago. However, the method for handling the black hole in the so-called moving puncture framework was discovered [14] (see also [15,16] for the original idea of the puncture framework). This framework enables one (even the beginner of numerical relativity) to perform a simulation for black hole spacetimes without special difficulty. (See also [17–19] for the progress in other approaches based on the black hole excision.) Soon after the discovery of the moving puncture framework, simulations for the merger of binary black holes [14] and black hole-neutron star binaries [4] have been performed.

Namely, it has already been possible to study most of the general relativistic astrophysical phenomena by numerical relativity, if an appropriate initial condition (and a supercomputer of certain power) is prepared. In this paper, we present a formulation for providing equilibrium states composed of a rotating black hole and self-gravitating torus in the puncture framework. We do not use the conformal flatness approximation because rapidly rotating black holes cannot be computed accurately with this approximation. With our formulation, equilibria of a rapidly rotating black hole and massive torus can be computed, as demonstrated in Sec. III. The solutions obtained in this method will be adopted for general relativistic simulation in the moving puncture framework and will be helpful for studying dynamical and astrophysical issues mentioned in the first paragraph.

It should be noted that equilibria of a black hole and torus was already computed by the pioneer work of Nishida and Eriguchi many years ago [20] and recently by Ansorg and Petroff [21]. In the present paper, we propose a different formulation from theirs in the puncture framework. In addition, we suggest different indicators of black hole mass from that used in [20,21] because the exact definition for a nonisolated black hole is still unknown and the previous one might not be a good indicator. We remark that characteristic physical properties of the black hole surrounded by massive torus we find are quite different from those reported previously. In our definition of black hole mass, the relations among the area, mass, and spin angular momentum of the black hole surrounded by massive torus are only slightly different from those of Kerr black holes. On the other hand, the relations of angular

velocity and surface gravity as functions of mass and spin are significantly different from those of Kerr black holes.

The paper is organized as follows. In Sec. II, we present our formulation for equilibria of rotating black hole-torus systems. Three candidates of the black hole mass in the presence of the torus are suggested. In Sec. III, numerical results in our formulation are presented paying attention to the properties of the black hole. Section IV is devoted to a summary. Throughout this paper, we adopt geometrical units in which $G = 1 = c$, where G and c denote the gravitational constant and the speed of light, respectively. Latin and Greek indices denote spatial and spacetime components.

II. FORMULATION

A. Basic equations

We derive the basic equations for a system of the rotating black hole and self-gravitating torus in axisymmetric equilibrium which are suitable for preparing initial data of the numerical relativity simulation in the moving puncture framework. First, we write the line element in the quasi-isotropic form [22–24]

$$ds^2 = -\alpha^2 dt^2 + \psi^4[e^{2q}(dr^2 + r^2 d\theta^2) + r^2 \sin^2\theta(\beta dt + d\varphi)^2], \quad (1)$$

where α is the lapse function, ψ is the conformal factor, β is the shift vector of the φ component, and e^{2q} denotes the conformal metric for the rr and $\theta\theta$ parts. These field variables are functions of r and θ. In this paper, the $3 + 1$ formalism of general relativity is used since our purpose is to prepare an initial condition for numerical relativity simulation.

In the following, we assume that the torus is composed of the perfect fluid for which the energy-momentum tensor is

$$T_{\mu\nu} = \rho h u_\mu u_\nu + P g_{\mu\nu}, \quad (2)$$

where ρ, h, u_μ, P, and $g_{\mu\nu}$ are the rest-mass density, specific enthalpy, four-velocity, pressure, and spacetime metric, respectively. In this paper, we adopt the polytropic equation of state (EOS)

$$P = K\rho^\Gamma, \quad (3)$$

where K and Γ are the polytropic and adiabatic constants, respectively. In this EOS, the specific internal energy ε and h are written by

$$\varepsilon = \frac{K}{\Gamma - 1}\rho^{\Gamma-1}, \quad (4)$$

$$h = 1 + \Gamma\varepsilon. \quad (5)$$

Nonzero components of the four-velocity are u^φ and u^t. The normalization relation $u^\mu u_\mu = -1$ gives the relation between them

$$(\alpha u^t)^2 = 1 + \frac{u_\varphi^2}{\psi^4 r^2 \sin^2\theta}. \quad (6)$$

From u_φ, the angular velocity Ω, defined by u^φ/u^t, is derived

$$\Omega = -\beta + \frac{u_\varphi}{\psi^4 u^t r^2 \sin^2\theta}. \quad (7)$$

In stationary axisymmetric spacetime, the Euler equation is integrated to give

$$\frac{h}{u^t} + \int h u_\varphi d\Omega = C, \quad (8)$$

where C is a constant (see Appendix A for the derivation of Eq. (8) and an extension of this relation in the presence of toroidal magnetic fields). Note that Eq. (8) holds irrespective of the chosen EOS as far as the fluid is isentropic.

In this paper, we choose the constant specific angular momentum as the rotation law, namely,

$$j \equiv h u_\varphi = \text{const.} \quad (9)$$

Then, the first integral of the Euler equation is

$$\frac{h}{u^t} + j\Omega = C, \quad (10)$$

or

$$\alpha\sqrt{h^2 + \frac{j^2}{\psi^4 r^2 \sin^2\theta}} - j\beta = C. \quad (11)$$

Equation (11) is the basic equation for providing h for given constants j and C. After h is obtained, ρ and P are determined using Eqs. (3) and (5) for given values of K and Γ.

We here choose the $j =$ constant law for simplicity (we do not consider astrophysical application of the equilibria computed below). An astrophysically realistic one would be different from this since tori of $j =$ constant law are known to be often unstable against nonaxisymmetric deformation and runaway collapse. In our formulation, equilibria can be computed with other rotation laws if they are written in the form $j = j(\Omega)$. In the numerical simulation which will be performed in the future, we will present equilibria in other rotation laws.

The basic equations for the metric functions are derived from the equations in the $3 + 1$ formalism of general relativity. Taking into account that the analytic solution for Kerr black holes in the puncture framework (and in the $3 + 1$ formalism) has been already found by Krivan and Price [25], we derive the basic equations based on their formulation in the following. The formulation derived in this strategy guarantees that in the zero limit of torus mass, the numerical solution automatically reduces to a Kerr solution.

In stationary axisymmetric spacetime with the line element (1), nonzero components of the extrinsic curvature

K_{ij} are $K_{r\varphi}$ and $K_{\theta\varphi}$. Defining the weighted extrinsic curvature,

$$\hat{K}_{ij} = \psi^2 K_{ij}, \tag{12}$$

the momentum constraint equation of a nontrivial component (φ component) is written as

$$\frac{1}{r^2}\frac{\partial(r^2\hat{K}_{r\varphi})}{\partial r} + \frac{1}{r^2\sin\theta}\frac{\partial(\sin\theta\hat{K}_{\theta\varphi})}{\partial\theta} = 8\pi T^t_\varphi \alpha\psi^6 e^{2q}. \tag{13}$$

Because the momentum constraint is linear in $\hat{K}_{ij}$, the nonzero components may be split as

$$\hat{K}_{r\varphi} = \frac{H_E\sin^2\theta}{r^2} + \frac{\psi^6}{2\alpha}r^2\sin^2\theta\partial_r\beta_{\rm T}, \tag{14}$$

$$\hat{K}_{\theta\varphi} = \frac{H_F\sin\theta}{r} + \frac{\psi^6}{2\alpha}r^2\sin^2\theta\partial_\theta\beta_{\rm T}, \tag{15}$$

where the first term of each denotes the contribution from a rotating black hole and the second term is that from a torus. $\beta_{\rm T}$ is the shift vector associated with the torus and equal to $\beta - \beta_{\rm K}$ where $\beta_{\rm K}$ is derived from

$$\frac{\partial\beta_{\rm K}}{\partial r} = \frac{2H_E\alpha}{r^4\psi^6}. \tag{16}$$

H_E and H_F satisfy a relation derived from the momentum constraint as [23]

$$r\frac{\partial H_E}{\partial r}\sin^3\theta + \frac{\partial H_F\sin^2\theta}{\partial\theta} = 0. \tag{17}$$

We assign the solutions for Kerr black holes to H_E and H_F [see Eqs. (36) and (37)]. Then, $\beta_{\rm K}$ is equal to the shift vector of the Kerr black hole in the absence of the torus.

Using the evolution equation for $\mathrm{tr}(K_{ij})$, the Hamiltonian constraint, and the momentum constraint, the equations for $\Phi \equiv \alpha\psi$, ψ, and $\beta_{\rm T}$ are derived as

$$\Delta\Phi = \frac{\Phi e^{2q}\tilde{R}}{8} + 2\pi(\rho_{\rm H} + 2S)\Phi e^{2q}\psi^4 + \frac{7A^2\Phi}{4\psi^8}, \tag{18}$$

$$\Delta\psi = \frac{\psi e^{2q}\tilde{R}}{8} - 2\pi\rho_{\rm H}e^{2q}\psi^5 - \frac{A^2}{4\psi^7}, \tag{19}$$

$$\Delta\beta_{\rm T} + \left(\frac{2}{r} + \frac{7}{\psi}\frac{\partial\psi}{\partial r} - \frac{1}{\Phi}\frac{\partial\Phi}{\partial r}\right)\frac{\partial\beta_{\rm T}}{\partial r} + \frac{1}{r^2}\left(2\cot\theta + \frac{7}{\psi}\frac{\partial\psi}{\partial\theta} - \frac{1}{\Phi}\frac{\partial\Phi}{\partial\theta}\right)\frac{\partial\beta_{\rm T}}{\partial\theta} = \frac{16\pi\alpha e^{2q}J}{r^2\sin^2\theta}, \tag{20}$$

where

$$A^2 \equiv \frac{\hat{K}^2_{r\varphi}}{r^2\sin^2\theta} + \frac{\hat{K}^2_{\theta\varphi}}{r^4\sin^2\theta}, \tag{21}$$

$$\rho_{\rm H} \equiv \alpha^2 T^{tt} = \rho h(\alpha u^t)^2 - P, \tag{22}$$

$$J \equiv \alpha T^t_\varphi = \rho\alpha u^t j, \tag{23}$$

$$S \equiv (\psi^2 r\sin\theta)^{-2}T_{\varphi\varphi} = \rho h[(\alpha u^t)^2 - 1] + 3P, \tag{24}$$

and $\tilde{R}$ is the Ricci scalar with respect to the conformal three-metric

$$\tilde{R} = -2e^{-2q}\left(\frac{\partial^2}{\partial r^2} + \frac{1}{r}\frac{\partial}{\partial r} + \frac{1}{r^2}\frac{\partial^2}{\partial\theta^2}\right)q. \tag{25}$$

Δ denotes the flat Laplacian,

$$\Delta = \frac{\partial^2}{\partial r^2} + \frac{2}{r}\frac{\partial}{\partial r} + \frac{1}{r^2}\left(\frac{\partial^2}{\partial\theta^2} + \cot\theta\frac{\partial}{\partial\theta}\right). \tag{26}$$

The equation for q is derived from the evolution equations for K_{ij}. In the present case, the evolution equation leads to

$$I_{ij} \equiv \alpha R_{ij} - 2\alpha K_{il}K^l{}_j - D_iD_j\alpha + K_{im}\frac{\partial\beta^m}{\partial x^j} + K_{jm}\frac{\partial\beta^m}{\partial x^i} - 8\pi\alpha\left[S_{ij} + \frac{1}{2}\gamma_{ij}(\rho_{\rm H} - S)\right] = 0, \tag{27}$$

where R_{ij} and D_i are the Ricci tensor and covariant derivative with respect to the three-metric γ_{ij}, and $S_{ij} = \rho h u_i u_j + P\gamma_{ij}$. Then, from the relation

$$I_{rr} + \frac{I_{\theta\theta}}{r^2} - \frac{3e^{2q}I_{\varphi\varphi}}{r^2\sin^2\theta} = 0, \tag{28}$$

an elliptic-type equation of q is derived:

$$\left(\frac{\partial^2}{\partial r^2} + \frac{1}{r}\frac{\partial}{\partial r} + \frac{1}{r^2}\frac{\partial^2}{\partial\theta^2}\right)q = -8\pi e^{2q}\left[\psi^4 P - \frac{\rho h u_\varphi^2}{r^2\sin^2\theta}\right] + \frac{3A^2}{\psi^8} + 2\left(\frac{1}{r}\frac{\partial}{\partial r} + \frac{\cot\theta}{r^2}\frac{\partial}{\partial\theta}\right)\times\ln(\Phi\psi) + \frac{4}{\Phi\psi}\left(\frac{\partial\Phi}{\partial r}\frac{\partial\psi}{\partial r} + \frac{1}{r^2}\frac{\partial\Phi}{\partial\theta}\frac{\partial\psi}{\partial\theta}\right). \tag{29}$$

Substituting Eq. (29) into Eq. (19), the equation for ψ is rewritten as

$$\Delta\psi = -2\pi\left[\rho_{\rm H} - P + \frac{\rho h u_\varphi^2}{\psi^4 r^2\sin^2\theta}\right]e^{2q}\psi^5 - \frac{A^2}{\psi^7} - \frac{\psi}{2}\left(\frac{1}{r}\frac{\partial}{\partial r} + \frac{\cot\theta}{r^2}\frac{\partial}{\partial\theta}\right)\ln(\Phi\psi) - \frac{1}{\Phi}\left(\frac{\partial\Phi}{\partial r}\frac{\partial\psi}{\partial r} + \frac{1}{r^2}\frac{\partial\Phi}{\partial\theta}\frac{\partial\psi}{\partial\theta}\right), \tag{30}$$

Using Eqs. (18), (19), (25), and (29), we find that $\Phi\psi$ obeys a simple equation

$$\left(\Delta + \frac{1}{r}\frac{\partial}{\partial r} + \frac{\cot\theta}{r^2}\frac{\partial}{\partial\theta}\right)(\Phi\psi) = 16\pi\Phi\psi^5 e^{2q}P. \quad (31)$$

Hence, it is better to choose this equation instead of that for Φ as one of basic equations.

If H_E and H_F are chosen to be equal to those of a Kerr black hole, the derived equations satisfy the Kerr solution in the quasi-isotropic coordinate in the absence of the torus. The specific forms are [25]

$$\alpha_{\rm K} = \sqrt{\frac{\Sigma_{\rm K}\Delta_{\rm K}}{(r_{\rm K}^2 + a^2)\Sigma_{\rm K} + 2ma^2 r_{\rm K}\sin^2\theta}}, \quad (32)$$

$$\beta_{\rm K} = -\frac{2mar_{\rm K}}{(r_{\rm K}^2 + a^2)\Sigma_{\rm K} + 2ma^2 r_{\rm K}\sin^2\theta}, \quad (33)$$

$$\psi_{\rm K} = \frac{1}{r^{1/2}}\left(r_{\rm K}^2 + a^2 + \frac{2ma^2 r_{\rm K}\sin^2\theta}{\Sigma_{\rm K}}\right)^{1/4}, \quad (34)$$

$$e^{q_{\rm K}} = \frac{\Sigma_{\rm K}}{\sqrt{(r_{\rm K}^2 + a^2)\Sigma_{\rm K} + 2ma^2 r_{\rm K}\sin^2\theta}}, \quad (35)$$

$$H_E = \frac{ma[(r_{\rm K}^2 - a^2)\Sigma_{\rm K} + 2r_{\rm K}^2(r_{\rm K}^2 + a^2)]}{\Sigma_{\rm K}^2}, \quad (36)$$

$$H_F = \frac{-2ma^3 r_{\rm K}\Delta_{\rm K}^{1/2}\cos\theta\sin^2\theta}{\Sigma_{\rm K}^2}, \quad (37)$$

where m and $a(|a| < m)$ are the mass and spin parameter of the Kerr black hole, $r_{\rm K}$ is the radial coordinate in the Boyer-Lindquist coordinate, and

$$\Sigma_{\rm K} = r_{\rm K}^2 + a^2\cos^2\theta, \quad (38)$$

$$\Delta_{\rm K} = r_{\rm K}^2 - 2mr_{\rm K} + a^2. \quad (39)$$

The relation between r and $r_{\rm K}$ [25] is

$$r_{\rm K} = r\left(1 + \frac{m}{r} + \frac{m^2 - a^2}{4r^2}\right), \quad (40)$$

or equivalently

$$r = \frac{r_{\rm K} - m + \Delta_{\rm K}^{1/2}}{2}. \quad (41)$$

We derive the equations for the field variables in the puncture framework [15]. This is possible because the elliptic operator for ψ and Φ in the basic equations are the flat operator. Assuming that the puncture is located at $r = 0$, we write ψ and Φ in the form

$$\psi = \left(1 + \frac{r_{\rm s}}{r}\right)e^{\phi}, \quad (42)$$

$$\Phi = \left(1 - \frac{r_{\rm s}}{r}\right)e^{-\phi}B, \quad (43)$$

where $r_{\rm s}$ is set to be $\sqrt{m^2 - a^2}/2$ following [25], and ϕ and B are new functions of r and θ. Using Eqs. (42) and (43), the elliptic-type equations for ϕ, $B(= e^b)$, $\beta_{\rm T}$, and q are rewritten as

$$\left[\frac{\partial^2}{\partial r^2} + \frac{2r}{r^2 - r_{\rm s}^2}\frac{\partial}{\partial r} + \frac{1}{r^2}\left(\frac{\partial^2}{\partial\theta^2} + \cot\theta\frac{\partial}{\partial\theta}\right)\right]\phi = -2\pi e^{2q}\psi^4\left[\rho_{\rm H} - P + \frac{\rho h u_\varphi^2}{\psi^4 r^2\sin^2\theta}\right] - \frac{A^2}{\psi^8} - \frac{\partial\phi}{\partial r}\frac{\partial b}{\partial r} - \frac{1}{r^2}\frac{\partial\phi}{\partial\theta}\frac{\partial b}{\partial\theta} - \frac{1}{2}\left[\frac{r - r_{\rm s}}{r(r + r_{\rm s})}\frac{\partial b}{\partial r} + \frac{\cot\theta}{r^2}\frac{\partial b}{\partial\theta}\right] \equiv S_\phi, \quad (44)$$

$$\left[\frac{\partial^2}{\partial r^2} + \frac{3r^2 + r_{\rm s}^2}{r(r^2 - r_{\rm s}^2)}\frac{\partial}{\partial r} + \frac{1}{r^2}\left(\frac{\partial^2}{\partial\theta^2} + 2\cot\theta\frac{\partial}{\partial\theta}\right)\right]B = 16\pi B e^{2q}\psi^4 P, \quad (45)$$

$$\left[\frac{\partial^2}{\partial r^2} + \left(\frac{4r^2 - 8r_{\rm s}r + 2r_{\rm s}^2}{r(r^2 - r_{\rm s}^2)} + 8\frac{\partial\phi}{\partial r} - \frac{\partial b}{\partial r}\right)\frac{\partial}{\partial r} + \frac{1}{r^2}\left\{\frac{\partial^2}{\partial\theta^2} + \left(3\cot\theta + 8\frac{\partial\phi}{\partial\theta} - \frac{\partial b}{\partial\theta}\right)\frac{\partial}{\partial\theta}\right\}\right]\beta_{\rm T} = \frac{16\pi\alpha e^{2q}J}{r^2\sin^2\theta}, \quad (46)$$

$$\left(\frac{\partial^2}{\partial r^2} + \frac{1}{r}\frac{\partial}{\partial r} + \frac{1}{r^2}\frac{\partial^2}{\partial\theta^2}\right)q = -8\pi e^{2q}\left[\psi^4 P - \frac{\rho h u_\varphi^2}{r^2\sin^2\theta}\right] + \frac{3A^2}{\psi^8} + 2\left(\frac{r - r_{\rm s}}{r(r + r_{\rm s})}\frac{\partial}{\partial r} + \frac{\cot\theta}{r^2}\frac{\partial}{\partial\theta}\right)b + \left[\frac{8r_{\rm s}}{r^2 - r_{\rm s}^2} + 4\frac{\partial(b - \phi)}{\partial r}\right]\frac{\partial\phi}{\partial r} + \frac{4}{r^2}\frac{\partial\phi}{\partial\theta}\frac{\partial(b - \phi)}{\partial\theta} \equiv S_q. \quad (47)$$

The equation for β_K is

$$\frac{\partial \beta_K}{\partial r} = 2H_E B e^{-8\phi} \frac{(r - r_s) r^2}{(r + r_s)^7}. \tag{48}$$

Equations (44)–(48) are the basic field equations to be solved in the puncture framework.

B. Boundary conditions

Although the basic equations (44)–(48) are written in the puncture framework, they also have an inversion symmetry with respect to the two-surface of $r = r_s$. In the absence of the torus, this is easily found by the coordinate transformation

$$\bar{r} = \frac{r_s^2}{r}. \tag{49}$$

Namely, the equations obtained by the transformation of (49) are identical with those obtained by simply changing the variable from r to $\bar{r}$. This implies that the following relations hold:

$$\phi(r) = \phi(\bar{r}), \tag{50}$$

$$B(r) = B(\bar{r}), \tag{51}$$

$$\beta_T(r) = \beta_T(\bar{r}), \tag{52}$$

$$\beta_K(r) = \beta_K(\bar{r}), \tag{53}$$

$$q(r) = q(\bar{r}). \tag{54}$$

Even in the presence of the torus, the inversion symmetry holds if we assume the relations

$$\rho(r) = \rho(\bar{r}), \tag{55}$$

$$u_\varphi(r) = -u_\varphi(\bar{r}), \tag{56}$$

$$u^t(r) = -u^t(\bar{r}). \tag{57}$$

The minus sign for the second and third relations comes from the fact that $\alpha(r) = -\alpha(\bar{r})$.

Assuming the presence of the inversion-symmetry relations for the matter (55)–(57), Eqs. (44)–(47) may be solved only for the region $r_s \le r < \infty$ with the boundary conditions at $r = r_s$

$$\frac{\partial \phi}{\partial r} = \frac{\partial B}{\partial r} = \frac{\partial \beta_T}{\partial r} = \frac{\partial q}{\partial r} = 0. \tag{58}$$

Then, the solutions for $r < r_s$ are obtained from Eqs. (50)–(54) with $\bar{r} > r_s$. The topology of the spacetime considered here is schematically described in Fig. 1.

The boundary conditions for $r \to \infty$ are

$$\phi \to \frac{M_1}{2r}, \tag{59}$$

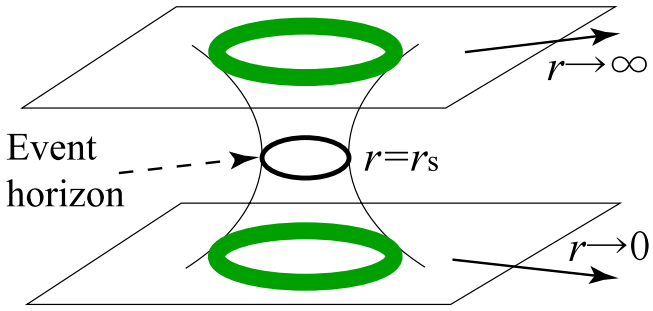

FIG. 1 (color online). Schematic picture for topology of the black hole-torus system considered in this paper. The thin and thick circles denote the event horizon and torus.

$$B \to -\frac{B_1}{r^2}, \tag{60}$$

$$\beta_T \to -\frac{2J_1}{r^3}, \tag{61}$$

$$q \to \frac{q_1 \sin^2\theta}{r^2}, \tag{62}$$

where M_1, B_1, J_1, and q_1 are constants. M_1 and J_1 may be used for deriving the total mass and angular momentum of the system (see Sec. II C). They are computed from

$$M_1 = -2 \int_{r_s}^{\infty} (r^2 - r_s^2) dr \int_0^{\pi/2} \sin\theta d\theta S_\phi, \tag{63}$$

$$J_1 = 4\pi \int_{r_s}^{\infty} r^2 dr \int_0^{\pi/2} \sin\theta d\theta \rho \alpha u^t \psi^6 e^{2q} j. \tag{64}$$

We note that these boundary conditions are physically the same as those in [24].

Note that q should be zero along the rotation axis because of the regularity there. This is reflected in the boundary condition (62). Another point which should be kept in mind is that the asymptotic behavior of the homogeneous solution for q is proportional to $\ln r$. In spite of this fact, the asymptotic behavior (62) has to be satisfied. This requires the relation

$$\int_{r_s}^{\infty} r dr \int_0^{\pi/2} d\theta S_q = 0. \tag{65}$$

Equation (65) is known as a virial identity introduced by Bonazzola and Gourgoulhon [26]. This identity is useful for checking accuracy of numerical results. We note that there is the other virial identity. We describe it in Sec. II C [see Eq. (95)].

Because the inversion-symmetric boundary condition is imposed, the two-surface of $r = r_s$ satisfies the relation for the apparent horizon, which agrees with the event horizon in the stationary spacetime [27]. The angular velocity of the event horizon should be equal to $-\beta$ [28], and hence, β at $r = r_s$ should be constant. This is guaranteed in the

present formulation as proven in the following: For β to be constant, $\partial\beta/\partial\theta$ has to be zero at $r = r_s$. From Eq. (20), we find that it is equivalent to the following condition because $\partial\beta/\partial r = 0$ at $r = r_s$:

$$\frac{\partial}{\partial r}\left(\frac{1}{\alpha}\frac{\partial\beta}{\partial r}\right) = 0. \tag{66}$$

For this equation to be satisfied, $\partial\beta/\partial r$ near $r = r_s$ has to satisfy

$$\frac{\partial\beta}{\partial r} = C_\beta\alpha\{1 + O[(r - r_s)^2]\}, \tag{67}$$

where C_β is a constant. Namely, the terms proportional to $\alpha \times (r - r_s)$ should be vanishing. This is indeed guaranteed in the present formulation because α and β satisfy inversion asymmetry and symmetry with respect to the $r = r_s$ surface, respectively. Therefore, β is constant on the event horizon. Numerical results also show that this is the case.

In solving the equation for β_T, we have to be careful about the boundary condition at $r = r_s$. The inversion-symmetric condition requires

$$\beta_T = \beta_{T0} + \beta_{T2}(r - r_s)^2 + O[(r - r_s)^4], \tag{68}$$

where β_{T0} and β_{T2} are constants. Substituting this relation into Eq. (46), it is found that these two constants cannot be determined. This implies that they are homogeneous components and can be arbitrarily given. To eliminate such components, we impose the boundary condition

$$\beta_T = O[(r - r_s)^4]. \tag{69}$$

In this boundary condition, the angular velocity and angular momentum of black holes are not affected by β_T (see Sec. II C).

Equation (48) is an ordinary differential equation of first order. A solution of this is derived by integration with the boundary condition at $r \to \infty$ as $\beta_K \to 0$. Specifically, the integration is carried out from $r = r_s$ toward infinity with an arbitrary initial value (we usually choose the value of the Kerr black hole for given mass m and spin a). Then, the value of β_K for $r \gg m$ approaches to a constant. Subtraction of this constant from the numerical solution results in a solution because Eq. (48) is linear in β_K.

Before closing this section, we note the following. Because of the presence of the inversion symmetry, the equations are solved for an excised region of $r \geq r_s$ in the present formulation. In this sense, the computation is performed using the excision technique. However, the basic equations are written in the puncture framework. Thus, the numerical solutions for the puncture framework (i.e., the solutions for the whole region) are easily reconstructed from the obtained solution of inversion symmetry. Such a solution can be used as initial data for numerical simulation in the moving puncture framework.

C. Quantities of black hole, torus, and system

The properties of a black hole surrounded by torus are analyzed from the quantities on the event horizon (i.e., on the two-surface of $r = r_s$). Specifically, a Komar-charge M_H, angular momentum J_H, the area A_H, proper length along a constant meridian C_p, circumference along the equatorial surface C_e, angular velocity Ω_H, and surface gravity κ of a black hole are computed from

$$M_H = \int_0^{\pi/2} \psi^2 r^2 \frac{\partial\alpha}{\partial r} \sin\theta d\theta + 2\Omega_H J_H, \tag{70}$$

$$J_H = \frac{1}{4}\int_0^{\pi/2} \frac{r^4\psi^6}{\alpha}\frac{\partial\beta}{\partial r}\sin^3\theta d\theta, \tag{71}$$

$$A_H = 4\pi\int_0^{\pi/2} \psi^4 e^q r^2 \sin\theta d\theta, \tag{72}$$

$$C_p = 4r_s\int_0^{\pi/2} \psi^2 e^q d\theta, \tag{73}$$

$$C_e = 2\pi r_s \psi(\theta = \pi/2)^2, \tag{74}$$

$$\Omega_H = -\beta = -\beta_K = \text{const}, \tag{75}$$

$$\kappa = \frac{\partial\alpha}{\partial r}\psi^{-2}e^{-q} = \frac{Be^{-4\phi-q}}{8r_s} = \text{const}. \tag{76}$$

M_H, J_H, Ω_H, and κ are defined according to the formula by Bardeen, Carter, and Hawking [24,28], and obey the Smarr relation [29]

$$M_H = \frac{\kappa}{4\pi}A_H + 2\Omega_H J_H. \tag{77}$$

In the absence of a torus (i.e. for a Kerr black hole),

$$M_H = m, \tag{78}$$

$$J_H = ma, \tag{79}$$

$$A_H = 8\pi m^2(1 + \sqrt{1 - a^2/m^2}), \tag{80}$$

$$\Omega_H = a/2mr_+, \tag{81}$$

$$\kappa = \sqrt{m^2 - a^2}/2mr_+, \tag{82}$$

$$C_e = 4\pi m, \tag{83}$$

where $r_+ = m + \sqrt{m^2 - a^2}$ is the radial coordinate of the event horizon in the Boyer-Lindquist coordinate. It is worthy to note that C_e (as well as M_H) for Kerr black holes is independent of spin a. Thus, the mass of the black hole may be determined from $C_e/4\pi$ in the absence of the torus. Even in the presence of the torus, this quantity may be useful for approximately determining black hole mass (at

least for the case that mass of the torus is much smaller than the black hole mass). Thus, we define

$$M_C \equiv \frac{C_e}{4\pi} \tag{84}$$

as a measure of black hole mass.

In the present choice of the boundary condition for β at $r = r_s$, $J_{\rm H}$ is always ma irrespective of the mass and spin of torus. On the other hand, $M_{\rm H}$, $A_{\rm H}$, κ, and $\Omega_{\rm H}$ depend on the property of the torus.

As pointed out in [24], the Komar-charge $M_{\rm H}$, defined by the surface integral on the event horizon, may or may not be a good indicator of the black hole mass in the presence of the torus. In [20,30] it is regarded as the black hole mass but no justification is shown. It may be nothing but a characteristic charge of mass dimension. Indeed, the numerical results shown below (see the discussion associated with Fig. 4, and also see the results shown in [30]) suggest that $M_{\rm H}$ might not be a good indicator of the black hole mass.

On the other hand, the area is a physical quantity, which is related to the irreducible mass [27] by

$$M_{\rm irr} = \sqrt{\frac{A_{\rm H}}{16\pi}}. \tag{85}$$

Also, in axisymmetric spacetimes, $J_{\rm H}$ is regarded as the angular momentum of a black hole [24]. Thus, remembering the following formula held for Kerr black holes,

$$2M_{\rm irr}^2 = m^2 + m\sqrt{m^2 - a^2}, \tag{86}$$

the mass of a black hole may be approximately estimated by the Christodoulou's formula [31]

$$M_{\rm BH} = M_{\rm irr}\sqrt{1 + \frac{J_{\rm H}^2}{4M_{\rm irr}^4}}. \tag{87}$$

In Sec. III, we compare $M_{\rm H}$, M_C, and $M_{\rm BH}$.

The rest-mass M_* and the angular momentum J_* of the torus are defined by

$$M_* = 4\pi \int_{r_s}^{\infty} r^2 dr \int_0^{\pi/2} \sin\theta d\theta \rho_*, \tag{88}$$

$$J_* = 4\pi \int_{r_s}^{\infty} r^2 dr \int_0^{\pi/2} \sin\theta d\theta \rho_* j, \tag{89}$$

where ρ_* is the rest-mass density defined by

$$\rho_* \equiv \rho \alpha u^t \psi^6 e^{2q}. \tag{90}$$

J_* is equal to J_1, and to $M_* j$ for the rotation profile of $j =$ const.

The total gravitational mass M and angular momentum J of the system are computed from the Komar integral [24]

$$M = M_{\rm H} + M_{\rm T}, \tag{91}$$

$$J = J_{\rm H} + J_*, \tag{92}$$

where

$$M_{\rm T} = 8\pi \int_{r_s}^{\infty} r^2 dr \int_0^{\pi/2} \sin\theta d\theta \times \left(-T_t^t + \frac{1}{2} T_\mu^\mu\right) \alpha \psi^6 e^{2q}. \tag{93}$$

The mass of the system is also computed from the Arnowitt-Deser-Misner (ADM) formula [32]. Using the asymptotic behavior of the three-metric, the ADM mass is calculated to be

$$M_{\rm ADM} = \sqrt{m^2 - a^2} + M_1, \tag{94}$$

where M_1 is defined in Eq. (59). In the stationary spacetime, the virial relation $M = M_{\rm ADM}$, i.e.,

$$M_{\rm H} + M_{\rm T} = \sqrt{m^2 - a^2} + M_1 \tag{95}$$

has to be satisfied [33]. Thus, the accuracy of numerical results can be measured from the magnitude of $|1 - M/M_{\rm ADM}|$.

In addition, we define rotational kinetic, internal, and gravitational potential energy of the torus

$$T = 4\pi \int_{r_s}^{\infty} r^2 dr \int_0^{\pi/2} \sin\theta d\theta \frac{1}{2} \rho_* j \Omega, \tag{96}$$

$$U = 4\pi \int_{r_s}^{\infty} r^2 dr \int_0^{\pi/2} \sin\theta d\theta \rho_* \varepsilon, \tag{97}$$

$$W = M_{\rm ADM} - M_{\rm BH} - M_* - T - U, \tag{98}$$

where $W < 0$. We note that in W, not only gravitational potential energy due to the self-gravity of the torus but also binding energy between the black hole and torus are included.

III. NUMERICAL COMPUTATION

A. Setting and calibration

Numerical computations were performed assuming the reflection symmetry with respect to the equatorial plane and the inversion symmetry with respect to the two-surface of $r = r_{\rm s}$. A nonuniform grid for r and a uniform grid for $\cos\theta$ are adopted with the fiducial grid size $(N_r, N_\theta) = (800, 100)$. Specifically, the grid is determined by

$$r_i = r_{\rm s} + \frac{f^i - 1}{f - 1}\Delta r, \quad \text{for } i = 1 \sim N_r, \tag{99}$$

$$\cos\theta_j = \frac{1}{N_\theta}\left(j - \frac{1}{2}\right) \quad \text{for } j = 1 \sim N_\theta. \tag{100}$$

Equation (99) implies that the radial grid spacing increases as $r_{i+1} - r_i = f(r_i - r_{i-1})$. The fiducial values of f and Δr are $f = 1.01$ and $r_s/50$. The outer boundaries are located at $r \sim 5700 r_s$ in this setting.

The numerical scheme is essentially the same as that used in [34]. Namely, we iteratively solve the field equations (44)–(48) as the boundary value problem and determine the density of the torus from the first integral of the Euler equation (11). For a numerical solution of the field equations, we used the second-order finite-differencing schemes.

As the first test of our numerical code, we solved Eqs. (44), (47), and (48) in the absence of matter to examine if the numerical solution agrees with that of a Kerr black hole with a good accuracy. In Fig. 2, we show the relative error of the numerical solution of ϕ and q for $a = 0.99m$ with the grid settings (a) $(N_r, N_\theta, \Delta r/r_s) = (800, 100, 1/50)$, (b) (730, 100, 1/25), (c) (660, 100, 1/12.5), (d) (590, 100, 1/6.25), and (e) (1200, 100, 1/50). For (a)–(d), we chose $f = 1.01$ and for (e), $f = 1.006\,66$. For all the cases, the outer boundary is located at $\approx 5700 r_s$. Figure 2 shows that for our fiducial grid setting with $(N_r, N_\theta, \Delta r/r_s) = (800, 100, 1/50)$, the numerical error is smaller than $\sim 10^{-3}$ for $r \lesssim 100m$. In the vicinity of the black hole in which the grid spacing is smallest, the numerical error decreases approximately at second order and with the fiducial grid, the error is of $O(10^{-4})$. On the other hand, in the zone with $r \gtrsim 10m$, the numerical error is larger and the convergence is slow. One reason is that the grid spacing in the outer region is much larger than that in the inner region. Actually, in the case (e) for which the grid spacing is smaller than those for (a)–(d) in the outer region, the numerical error is suppressed (in particular for ϕ). The other reason is that the numerical error is systematically generated by the incomplete boundary conditions at the outer boundaries and along the symmetric axis: In our present treatment, the boundary conditions are imposed taking into account the behavior of the lowest-order multipole. This treatment restricts improving the accuracy beyond a certain level. To derive more accurate results, the higher-order multipoles should be taken into account with a better numerical approach (e.g., [35]). However, the numerical error $\sim 10^{-3}$ is small enough for the purpose of the present paper.

The tests were also performed changing N_θ. We found that the numerical results depend very weakly on it as far as $N_\theta \geq 100$. We also varied the value of a, and found that the magnitude and behavior of the numerical error are essentially the same as far as $|a/m|$ is not close to unity. For $|a| \to m$ (in the limit of the extreme Kerr solution), however, we found it difficult to get solutions. This is because of the fact that r_s approaches zero for $|a| \to m$ (i.e., the coordinate distance between the event horizon and the spatial infinity in the bottom-sheet world approaches zero); in such a case, resolving the region near the event horizon with $\Delta r \ll r_s$ requires a huge grid number. The present numerical approach is not suitable for such an extreme case.

Convergence of numerical solutions for different grid resolutions was also checked in the presence of the torus. We found that the numerical solutions for ϕ, B, and β converge approximately at second order. For that of q, the convergence is slow. This is probably because of the fact that an unphysical solution resulting from the insufficient boundary condition slightly contaminates the numerical solution. (Note that we have to exclude the homogeneous solution, $q \propto \ln r$, from the numerical solution for Eq. (47), but with the approximate boundary condition used in this work, such a homogeneous term is excluded in an insufficient way.) In Appendix B, we briefly describe the method for checking the convergence and present the results.

The accuracy of the numerical results for the black hole-torus system is measured from

$$\text{Error} = \frac{|\int_{r_s}^{\infty} r dr \int_0^{\pi/2} d\theta S_q|}{\int_{r_s}^{\infty} r dr \int_0^{\pi/2} d\theta \frac{3A^2}{\psi^8}}. \tag{101}$$

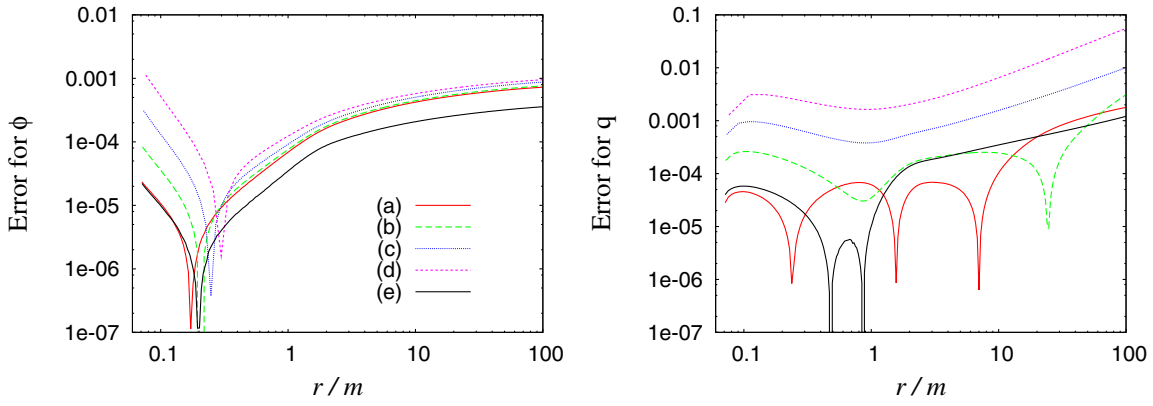

FIG. 2 (color online). The relative error of the numerical solutions of ϕ and q for the Kerr black hole with $a = 0.99m$ as a function of r/m in the equatorial plane. The solid, long-dashed, dotted, dashed, and thin solid curves denote the results for the grid settings (a)–(e), respectively.

This should be zero for the exact solution due to the virial identity (65) [26]. We found that the magnitude of "error" for the typical grid size is less than 0.1% and decreases with improving the grid resolution and with increasing the characteristic orbital radius of the torus.

We also checked if two masses M and $M_{\rm ADM}$ computed by Eqs. (91) and (94) agree each other. We found that they agree within $\sim 0.1\%$ error for most of the models. The exception is the case in which $a \gtrsim 0.9m$, $M_* \gtrsim m$, and the radius of the inner edge of the torus is close to that of the innermost stable circular orbit. In such a case, the error is $\sim 1\%$ in the typical grid size. Irrespective of a/m, the error slightly increases with M_* while it decreases with improving the grid resolution or with increasing the orbital radius of the torus. We note that we estimate the magnitude of the error for M_C, $M_{\rm H}$, and $M_{\rm BH}$ from the computations of different grid settings, and found that the error is much smaller than $|1 - M/M_{\rm ADM}|$ for the fiducial setting.

In numerical computation of an equilibrium sequence of the black hole-torus system, we first specify m and a. Here, m is a scaling parameter, i.e., all the quantities of mass and radius dimensions linearly increase with m. Thus, we simply set it to be unity. Since m and a are given, r_s is also fixed to be $\sqrt{m^2 - a^2}/2$. To efficiently see the effect of the torus on the properties of a black hole, tori of close orbits around rotating black holes are chosen in numerical computation. To specify a torus, we first give the coordinate radii of the inner and outer edges in the equatorial plane (denoted by r_1 and r_2), and ε at $r = 2r_1r_2/(r_1 + r_2)$ (denoted by ε_0). We chose the value of r_1 to be slightly larger than the radius of the innermost stable circular orbit around the black hole. With the increase of ε_0 for fixed values of r_1 and r_2, the mass of the torus increases.

Computations were performed for a wide variety of parameter sets (a, r_1, r_2). We found that numerical solutions can be obtained for a wide range of M_*/m as long as the black hole is not extremely rapidly rotating as $|a| \sim m$. In the present paper, we focus only on the case $|a| \leq 0.9m$ although we checked that the numerical computation is feasible even for $|a| = 0.995m$ in the fiducial grid setting. For $|a| \to m$, the properties of the black hole reported in Sec. III B might be modified, in particular, for a very compact torus of the inner edge close to the event horizon. We do not study such an extreme case in this paper.

In the following, we present numerical results for 7 parameter sets of $(a/m, r_1/m, r_2/m)$: (i) (0.9, 1.5, 20), (ii) (0.9, 5, 20), (iii) (0.9, 10, 20), (iv) (0.5, 3.5, 20), (v) (0.1, 5, 20), (vi) $(-0.5, 7, 20)$, and (vii) $(-0.9, 8, 20)$. Here, the negative value of a implies that the torus is counterrotating against the black hole. We compute sequences of equilibria changing the mass of torus while fixing m, a, r_1, and r_2.

We choose $\Gamma = 4/3$ polytropic EOS for the torus. This choice is reasonable because the torus around a black hole formed from stellar core collapse or merger of a black hole-neutron star binary is often hot and the pressure is dominated by degenerate pressure of relativistic electrons as well as by radiation pressure. Of course, a more realistic EOS will be necessary in considering an astrophysical application.

B. Results

In Fig. 3(a), we display the density contour curves for the case (i) with $M_*/m \approx 0.4$. It is found that the torus has a donut-shape with the maximum thickness comparable to the width $r_2 - r_1$. This is a universal feature that holds for

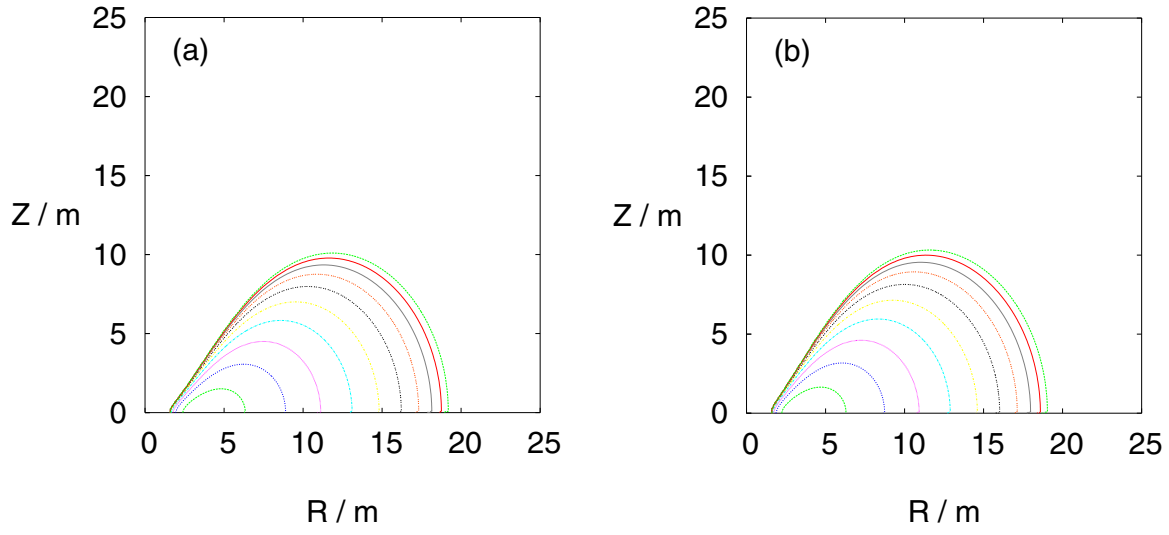

FIG. 3 (color online). (a) Density contours for the case (i) with $M_*/m = 0.400$. The contours are plotted for $\rho = 0.8\rho_{\rm max} \times 10^{i/2}$ where $i = 0$–9. The event horizon is located for $r \approx 0.218m$. (b) The same as (a) but for $a = 0.99m$. The event horizon is located for $r \approx 0.0705m$.

the $j =$ constant rotation profile. We note that for a profile in which j increases with the decrease of Ω, the thickness is not as wide as $r_2 - r_1$. In Fig. 3(b), we also display the density contour curves for $a = 0.99m$ with $M_*/m \approx 0.4$, $r_1 = 1.5m$, and $r_2 = 20m$ for demonstrating that the computation is feasible even for rapidly rotating black holes. Comparison of Fig. 3(a) and 3(b) shows that the density profile depends weakly on the value of a/m although for the larger value of a/m with given values of m, r_1, r_2, and M_*, the torus becomes more compact (i.e., the averaged value of the cylindrical radius is smaller).

The values of $|T/W|$ are always larger than 0.3 for compact tori considered in this paper. Because they are much larger than the well-known value for the onset of dynamical instability against nonaxisymmetric deformation $\sim$0.27 [36], equilibria are likely to be unstable. Exploring the nonaxisymmetric stability of such equilibria is an issue in the future. In the following, we focus on the study for the properties of black holes surrounded by a massive torus.

Figure 4 shows ϕ and $-\beta$ as functions of r in the equatorial plane for the case (i) with $M_*/m = 0.043$, 0.400, and 0.800 and for (v) with $M_*/m = 0.093$, 0.405, and 0.835. For the case (i) in which the black hole is rapidly rotating, the values of ϕ (and hence ψ) near the event horizon depends weakly on the mass of the torus. Because ψ primarily determines the strength of gravity, this suggests that the properties of the black hole depend weakly on the torus for (i).

For the case (v) in which the black hole is slowly rotating, the values of ϕ near the event horizon depend strongly on the mass of the torus (note that for $a = 0$, $\phi \to 0$ in the limit $M_* \to 0$). This is reflected in a sensitive dependence of the black hole mass on the torus mass (see Fig. 5). In this case, the magnitude of A^2 [cf. Eq. (21)] near the event horizon increases sensitively with M_* and with the angular momentum of the torus, because the angular momentum of the system is small in the absence of the torus. A^2 is not a local quantity and hence affects the gravity near the event horizon, resulting in the increase of the black hole mass. In other words, the properties of the black hole depend sensitively on the angular momentum of the torus if the black hole is slowly rotating.

For $r > r_1$, the magnitude of ϕ increases with M_* irrespective of the value of a. This is reflected in the increase of the total mass M. For the case of small values of a, the profile of ϕ is primarily determined by the torus for $M_* \sim m$ as shown in Fig. 4(c).

As in the case of ϕ, the magnitude of $|\beta|$ for $r > r_1$ increases with M_* reflecting the fact that the total angular momentum of the system increases. On the other hand, the

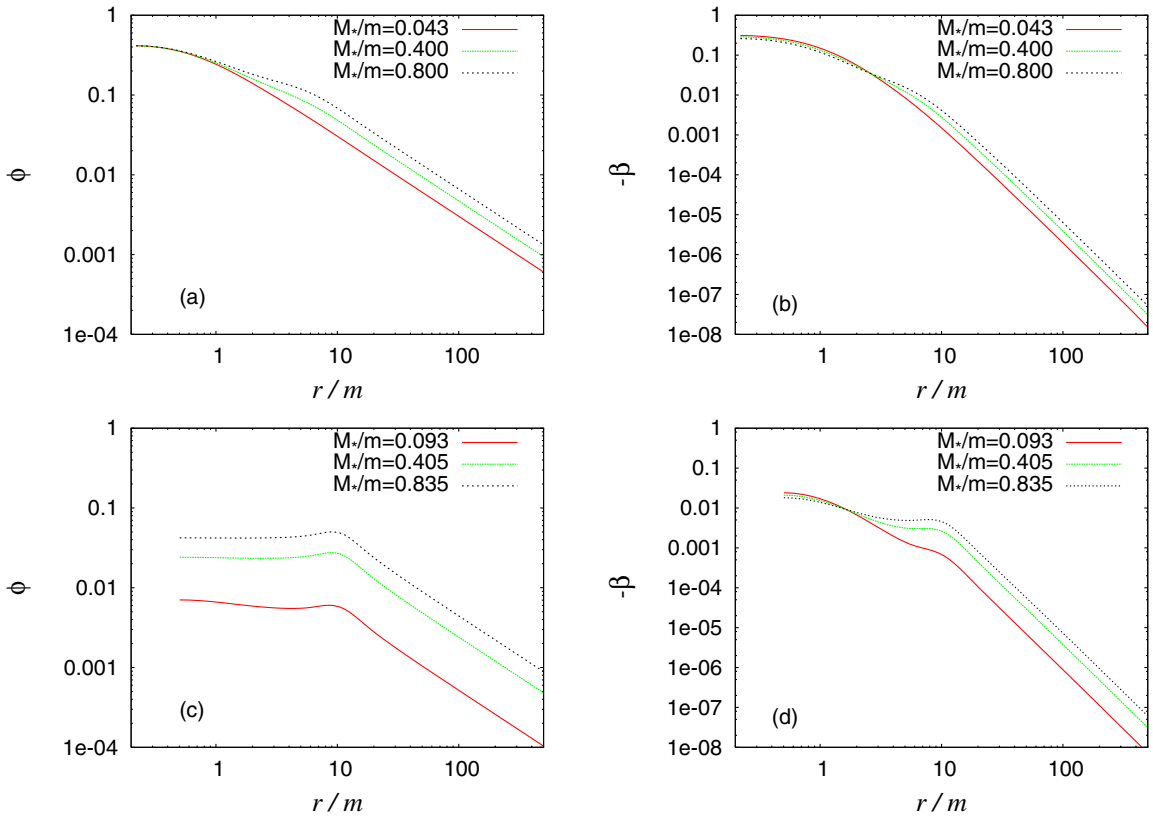

FIG. 4 (color online). ϕ and $-\beta$ as functions of r in the equatorial plane (a, b) for the case (i) with $M_*/m = 0.043$, 0.400, and 0.800 and (c, d) for the case (v) with $M_*/m = 0.093$, 0.405, and 0.835.

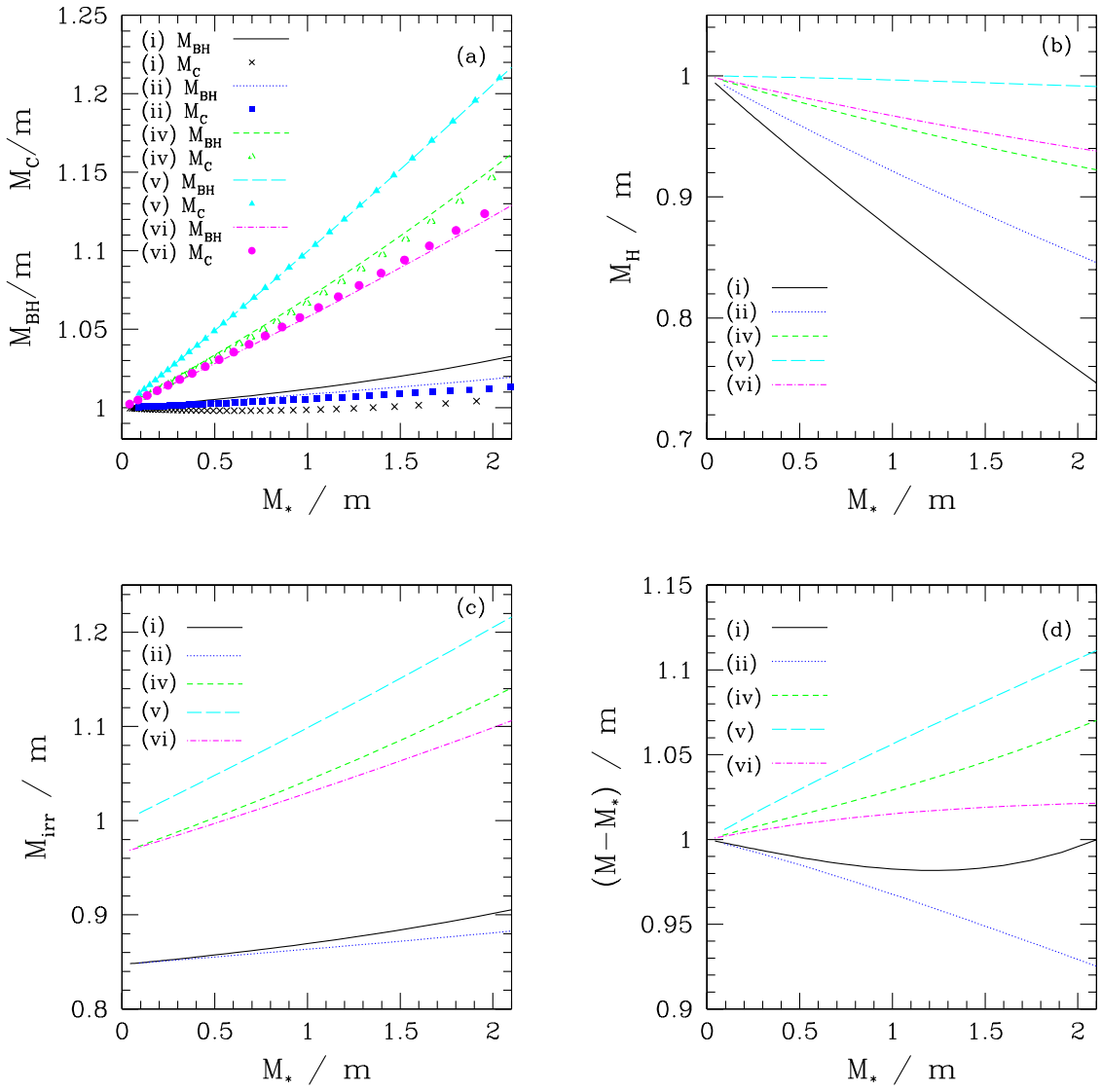

FIG. 5 (color online). (a) $M_{\rm BH}$ and $M_{\rm C}$ as functions of M_* for the cases (i), (ii), (iv), (v), (vi). (b) The same as (a) but for $M_{\rm H}$. (c) The same as (a) but for $M_{\rm irr}$. (d) The same as (b) but for $M - M_*$.

value of $|\beta|$ on the event horizon decreases with the increase of M_*, implying that the spin angular velocity of the black hole decreases [cf. Eq. (75)]. For the case (v), the magnitude of $|\beta|$ is much smaller than that for (i). Because of this, the profile of β is modified strongly by the angular momentum of the torus.

Figure 5 shows (a) $M_{\rm BH}$ and M_C, (b) $M_{\rm H}$, (c) $M_{\rm irr}$, and (d) $M - M_*$ as functions of M_*. Figure 5(a) indicates that $M_{\rm BH}$ and M_C coincide well. For the case (i) in which r_1 is very small and the black hole is rapidly rotating ($a = 0.9m$), the difference of two quantities is fairly large, but it is still at most $\sim 3\%$. The coincidence is very good for slightly larger values of r_1 (e.g., see the results for (ii) in which $a = 0.9m$ and $r_1/m = 5$), implying that the relatively poor coincidence occurs only for very small values of r_1. Remembering that M_C and $M_{\rm BH}$ are equal to the mass of Kerr black holes in the absence of the torus, the numerical results suggest that these two values may be approximately equal to the black hole mass even in the presence of the torus.

On the other hand, Fig. 5(b) shows that $M_{\rm H}$ *decreases* with the increase of M_*, and hence, disagrees considerably with $M_{\rm BH}$ and M_C. This raises a question that $M_{\rm H}$ might not be a good indicator of the black hole mass in the presence of the torus. In addition, there are two facts which suggest that $M_{\rm H}$ might not be a good indicator of the black hole mass. The first one is found from Figs. 5(b) and 5(c), which show that with the increase of $M_{\rm irr}$, $M_{\rm H}$ decreases for a given value of $J_{\rm H}$. In particular, $M_{\rm H}$ is smaller than $M_{\rm irr}$ for the case (i) with $M_* \gtrsim m$. If the black hole mass is assumed to be derived from the area by a formula similar to Eq. (80) even in the presence of the torus, $M_{\rm irr}$ should be smaller

than the black hole mass by definition of "irreducible" mass, and thus, $M_{\rm H}$ could not be the black hole mass at least for such a case. In order for $M_{\rm H}$ to be the black hole mass, the relation among the area, the mass, and the spin has to be significantly different from Eq. (80). In contrast, $M_{\rm BH}$ and M_C increase with $M_{\rm irr}$, and are always larger than $M_{\rm irr}$. If they were in approximate agreement with the black hole mass, the relation for the area will be similar to Eq. (80).

The second fact is found from the relation between $M - M_*$ and M_*. Because the black hole and torus constitute a bound system, the total mass of the system M should be smaller than the sum of M_* and black hole mass because of the presence of negative binding energy. This implies that $M - M_*$ should be smaller than the black hole mass. Comparing $M - M_*$ with $M_{\rm BH}$ or M_C by Figs. 5(a) and 5(d), we find that the relation $M - M_* < M_{\rm BH}$ or M_C always holds. By contrast, $M_{\rm H}$ is smaller than $M - M_*$. If $M_{\rm H}$ is the black hole mass, it is very difficult to physically explain this numerical result.

Figure 5 shows that $M_{\rm H}$ is smaller than $M_{\rm BH}$ and M_C by a factor $\sim 0.1 M_*$, which is of order of the absolute magnitude of binding energy between the black hole and torus. This suggests that $M_{\rm H}$ contains not only the component of bare black hole mass but also an amount of binding energy between the black hole and torus. This fact has been already pointed out in [24] briefly. In Appendix C, we clarify this point again, considering the Newtonian limit of Eq. (91).

In the following, we regard $M_{\rm BH}$ as the black hole mass. M_C may be a better measure than $M_{\rm BH}$, but these two approximately agree and the difference is at most $\sim 3\%$ even for the system of the very compact torus such as the case (i) and typically much smaller. In the analysis shown below, such a small difference does not change the conclusion.

In Fig. 6, we show a nondimensional spin parameter $J_{\rm H}/M_{\rm BH}^2$ as a function of M_* for the cases (i) and (iv)–(vii). Irrespective of the values of a, r_1, and r_2, the spin parameter decreases with the increase of M_*. This indicates that the black hole spin would never exceed unity. Comparing the results for (i) and (iii), we find that for the larger values of orbital radius of the torus, the change rate of the spin parameter ($|d(J_{\rm H}/M_{\rm BH}^2)/dM_*|$) is smaller. For $r_1/m \sim 10$, the black hole spin is modified at most $\sim 5\%$ even for $M_* \sim 2M_{\rm BH}$.

As found in [21], another nondimensional parameter $J_{\rm H}/M_{\rm H}^2$ exceeds unity for $a = 0.9m$ even with a small value of $M_* \gtrsim m$. However, there is no reason to believe that $M_{\rm H}$ is a good indicator of the black hole mass, as mentioned above. Hence, we do not consider $J_{\rm H}/M_{\rm H}^2$ as the spin parameter.

In Fig. 7, we show C_p/C_e as a function of $J_{\rm H}/M_{\rm BH}^2$ for the cases (i) and (iii)–(vii). Reflecting the fact that the spin parameter of the black hole decreases with the increase of M_*, so does C_p/C_e. It is also seen that the relation between C_p/C_e and the spin parameter is in a fair agreement with

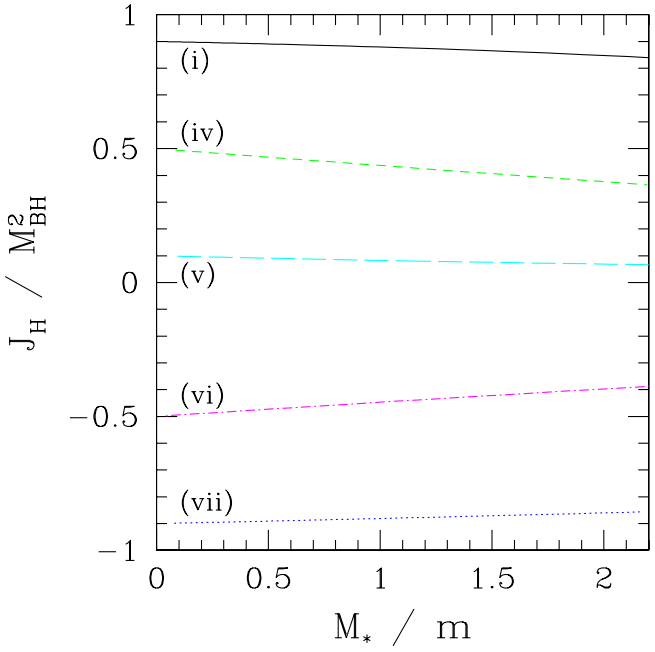

FIG. 6 (color online). $J_{\rm H}/M_{\rm BH}^2$ as a function of M_* for (i) and (iv)–(vii). The label of each curve denotes the model.

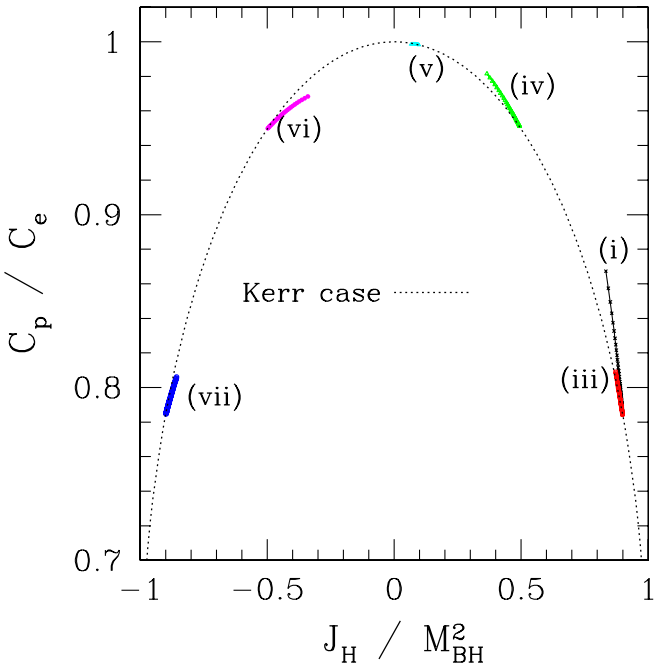

FIG. 7 (color online). C_p/C_e as a function of $J_{\rm H}/M_{\rm BH}^2$ for (i) and (iii)–(vii). For comparison, the relation for Kerr black holes is shown together (dotted curve). For $M_* \to 0$, the relation for C_p/C_e agrees with that of the Kerr black holes. With the increase of M_*, the relation slightly deviates from the dashed curve, but the difference is not very large. The data of $M_* \lesssim 2.3m$ are used for generating this figure.

that of Kerr black holes. In particular, the agreement is very good for $M_* < M_{\rm BH}$ or for $r_1 \gtrsim 10m$. This implies that the shape of the black holes is only weakly modified by the gravity of the torus. This result suggests that C_p/C_e could be used for approximately estimating the nondimensional spin parameter of black holes even in the presence of the torus.

Figure 8 shows $M_{\rm BH}\Omega_{\rm H}$ as a function of $J_{\rm H}/M_{\rm BH}^2$. Because the spin parameter decreases with the increase of M_*, it is natural that the absolute value of the angular velocity of the black hole also decreases. However, the decrease factor is beyond that expected from the relation of Kerr black holes. This is likely due to the presence of the angular momentum of the torus. Recall that the angular velocity of a rotating black hole is associated with the frame dragging due to its rotation. If a rotating black hole is surrounded by an object of slower or counterrotation, the frame dragging effect is weakened, and the angular velocity of the black hole should be decelerated. For the cases (vi) and (vii), the torus counterrotates around the black hole, and hence, the angular velocity of the black hole decreases with the increase of M_*. For (i)–(iv), the typical angular velocity of the torus is much smaller than that of the black hole. Therefore, a significant decrease of $\Omega_{\rm H}$ with the increase of M_* is reasonable. For (v), the angular velocity of the black hole is as slow as that of the torus. Reflecting this fact, the decrease factor of $\Omega_{\rm H}$ $(d\Omega_{\rm H}/dM_*)$ is much smaller than those of other cases.

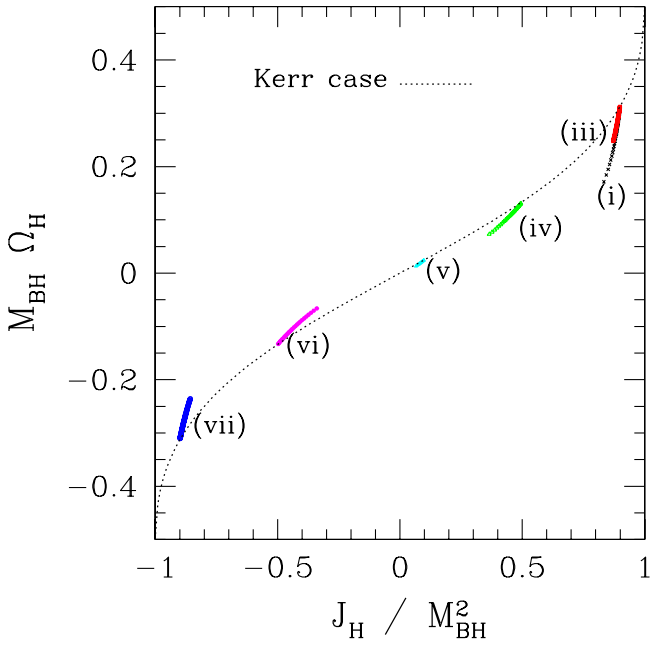

FIG. 8 (color online). $M_{\rm BH}\Omega_{\rm H}$ as a function of $J_{\rm H}/M_{\rm BH}^2$ for (i) and (iii)–(vii). The dotted curve denotes the relation for Kerr black holes. For $M_* = 0$, $|M_{\rm BH}\Omega_{\rm H}|$ agrees with that of the Kerr black holes, and for $M_* > 0$, it monotonically decreases with the increase of M_*. The data of $M_* \lesssim 2.3m$ are used for generating this figure.

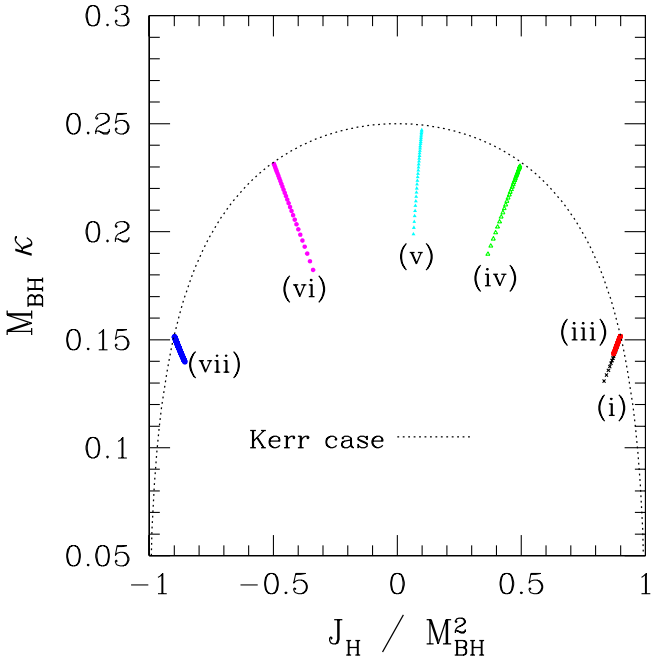

FIG. 9 (color online). $M_{\rm BH}\kappa$ as a function of $J_{\rm H}/M_{\rm BH}^2$ for (i) and (iii)–(vii). The dotted curve denotes the relation for Kerr black holes. For $M_* = 0$, $M_{\rm BH}\kappa$ agrees with that of Kerr black holes. With the increase of M_*, it monotonically decreases. The data of $M_* \lesssim 2.3m$ are used for generating this figure.

Figure 9 shows $M_{\rm BH}\kappa$ as a function of $J_{\rm H}/M_{\rm BH}^2$. It agrees with the value of the corresponding Kerr black hole in the limit $M_* \to 0$. However, it monotonically decreases with the increase of M_*, and hence, for a given spin parameter, it does not agree with the value of the Kerr black hole at all. This result is qualitatively consistent with the naive expectation because κ approximately denotes the strength of gravity on the event horizon and the magnitude of the surface gravity is likely to be weakened by a tidal force of the torus.

The decrease of κ with the increase of M_* correlates with the decrease of $M_{\rm H}$ [see Eq. (77) and Fig. 5(b)]. As we already mentioned, the decrease of $M_{\rm H}$ is likely to be attributed to the increase of the absolute magnitude of binding energy between the black hole and torus. Because both the absolute magnitude of the binding energy and tidal force of the torus increase with M_*, this correlation is quite reasonable.

Figure 10 shows the nondimensional spin parameter of the system J/M^2 as a function of M_*. For a small value of M_*, the angular momentum of the system is dominated by the black hole, but for a sufficiently large value, the torus determines it. As the mass of the torus increases, the spin parameter eventually reaches the maximum and then decreases. The reason of this behavior is that the torus becomes self-gravitating and the angular momentum is primarily determined by the mass-energy of the torus not by that of the black hole. In such a state, the ratio of

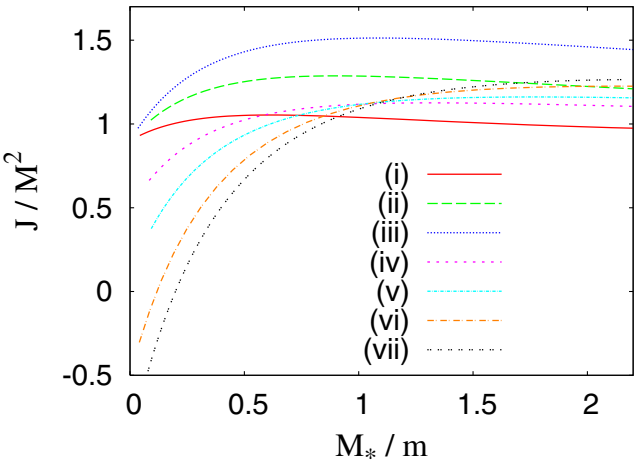

FIG. 10 (color online). The nondimensional spin parameter of the system J/M^2 as a function of M_*/m for (i)–(vii). Note that the compactness of the torus, M_*/r_c, is approximately proportional to M_*/m and hence for the large value of M_*/m, J/M^2 decreases with increasing the compactness.

rotational kinetic energy T to gravitational potential energy W of the torus depends weakly on its mass. The angular momentum of the torus is approximately proportional to T/Ω where Ω is the typical magnitude of the angular velocity of the torus which is approximately written for $M_* \gg M_{\rm BH} \sim m$ as

$$\Omega \sim \left(\frac{M_*}{r_c^3}\right)^{3/2}. \tag{102}$$

On the other hand, for $M_* \gg M_{\rm BH} \sim m$,

$$\frac{J}{M^2} \sim \frac{J_*}{M_*^2} \sim \frac{T}{M_*^2\Omega}, \tag{103}$$

whence

$$\frac{J}{M^2} \sim \frac{T}{W}\left(\frac{r_c}{M_*}\right)^{1/2}. \tag{104}$$

In the above estimate, we ignore coefficients of order unity. Equation (104) implies that for an approximately constant value of T/W, J/M^2 decreases with the increase of the compactness M_*/r_c for $M_* \gg M_{\rm BH}$, qualitatively explaining the behavior of Fig. 10.

For the high-mass models of the case (i), the spin parameter is smaller than unity. This indicates that even if a massive torus which is unstable against gravitational collapse is swallowed into the black hole, the final outcome will be a Kerr black hole of the spin parameter smaller than unity.

IV. SUMMARY

In this paper, we present a formulation for numerically computing an equilibrium system composed of a rotating black hole and a self-gravitating torus. Describing the black hole in the puncture framework, we derive basic equations for the equilibrium. It is shown that the resulting basic equations have an inversion symmetry with respect to the two-surface of the event horizon. Because of this property, the equations can be solved only for outside of the event horizon imposing the boundary condition at the event horizon. Then, the solutions for the inside are provided from the inversion-symmetric relations to constitute a puncture date. In our formulation, the spin angular momentum of the black hole is *a priori* specified. This is a good aspect for computing an equilibrium of a rapidly rotating black hole.

Numerical computations for equilibria were performed for a wide range of parameters. We showed that numerical solutions can be obtained for a rapidly rotating black hole with $a = 0.99m$ and for a wide range of mass ratio of the torus mass to the black hole mass. In addition, we illustrated several circumstantial facts which suggest that $M_{\rm H}$, a Komar-charge calculated from the surface integral on the event horizon, might not be a good indicator for the black hole mass in the presence of the torus. As alternatives, $M_{\rm BH}$ and M_C defined by Eqs. (84) and (87) were suggested for possible better indicators. Assuming that $M_{\rm BH}$ is the black hole mass, the properties of the black hole were investigated, and we found that they are quite different from those reported in the previous works [21]: In our definition of black hole mass, the relations among the area, mass, and spin angular momentum of the black hole are only slightly different from those of Kerr black holes even when the black hole is surrounded by a massive torus. However, it should be kept in mind that a conclusive definition of the black hole mass is still unknown. Searching for the mass formula of the black hole surrounded by matter is the issue for the future. This is the issue not only for the black hole-torus system but also for other systems such as black hole-neutron star binaries.

The numerical solutions can be used as an initial condition for the numerical relativity simulation in the moving puncture framework [4,14]. We plan to perform such a simulation for studying the nonaxisymmetric instability, magnetorotational instability, and runaway instability of the self-gravitating torus surrounding a rotating black hole. Such a system is a possible outcome formed after the stellar core collapse of massive star and after the merger of the black hole-neutron star binary. Numerical simulation will be helpful for getting insight on these phenomena. A simulation for a dense and hot torus with a sophisticated microphysics is also worthy to be done for modeling a dynamics of the central engine of gamma-ray bursts.

The present study may be the first step toward computation of a quasiequilibrium state for a binary of a rotating black hole and neutron star. We demonstrated that the exact equilibrium can be computed in the puncture framework for the axisymmetric system of the torus. In the black hole-neutron star binary, a similar method may be adaptable if

we do not assume the conformal flatness of the three-metric which has been often assumed for deriving quasie-quilibrium of compact binaries. In the axisymmetric case, the Laplace operator which appears in the elliptic-type equations for ψ and α reduces to the flat operator in the quasi-isotropic gauge. This enables one to use the puncture framework in a straightforward manner. In the black hole-neutron star case which is a nonaxisymmetric system, it is not trivial if such a convenient gauge is present or not. Exploring the gauge suitable for using the puncture method is an interesting issue.

ACKNOWLEDGMENTS

The author thanks K. Nakao and T. Shiromizu for conversation. This work was supported in part by Monbukagakusho Grant No. 17540232 and No. 19540263.

APPENDIX A: DERIVATION OF THE FIRST INTEGRAL OF THE EULER EQUATION

Appendix A is devoted to the derivation of the first integral of the Euler equation. It is possible to derive the relation even in the presence of toroidal magnetic fields for the ideal MHD fluid, and hence, we start with the energy-momentum tensor as

$$T_{\mu\nu} = (\rho h + b^2)u_\mu u_\nu + (P + \tfrac{1}{2}b^2)g_{\mu\nu} - b_\mu b_\nu, \quad \text{(A1)}$$

where b^μ is the spacetime-vector of magnetic fields and b^2 is its norm $b^\mu b_\mu$. In the ideal MHD approximation, the following relation holds:

$$b^\mu u_\mu = 0. \quad \text{(A2)}$$

Assuming that φ- and t-components are only nonzero components of u^μ and b^μ, we have the relation

$$b_t = -\frac{u^\varphi}{u^t} b_\varphi = -\Omega b_\varphi. \quad \text{(A3)}$$

Also, the continuity, energy, and induction equations become trivial equations, and hence, we only need to focus on the space-components of the Euler equation

$$\nabla_\mu T^\mu{}_k = 0, \quad \text{(A4)}$$

where ∇_μ is the covariant derivative with respect to $g_{\mu\nu}$.

In the stationary axisymmetric case of $u^r = u^\theta = b^r = b^\theta = 0$ with the quasi-isotropic gauge for $g_{\mu\nu}$, the Euler equation is written as

$$-\frac{1}{2}\left[(\rho h + b^2)u^\mu u^\nu - b^\mu b^\nu\right]\frac{\partial g_{\mu\nu}}{\partial x^k} + \frac{\partial}{\partial x^k}\left(P + \frac{1}{2}b^2\right) = 0. \quad \text{(A5)}$$

For $x^k = \varphi$, the equation is trivially satisfied, and hence, we only need to consider $x^k = r$ and θ. The first and second terms of Eq. (A5) are calculated from the relations

$$\frac{1}{2}u^\mu u^\sigma g_{\mu\sigma,k} = \frac{u^t{}_{,k}}{u^t} - u^t u_\varphi \Omega_{,k}, \quad \text{(A6)}$$

$$\frac{1}{2}b^\mu b^\sigma g_{\mu\sigma,k} = b^2\left[\frac{u^t{}_{,k}}{u^t} + \frac{D_{,k}}{2D} - u^t u_\varphi \Omega_{,k}\right], \quad \text{(A7)}$$

where

$$D = |g_{tt}g_{\varphi\varphi} - g_{t\varphi}^2| = \alpha^2\psi^4 r^2 \sin^2\theta, \quad \text{(A8)}$$

and for deriving Eq. (A7), we used the relation (A3) and $b_\varphi^2 = D(u^t)^2 b^2$. Using Eqs. (A6) and (A7), we reach

$$h\left(u^t u_\varphi \Omega_{,k} - \frac{u^t_{,k}}{u^t}\right) + \frac{P_{,k}}{\rho} + \frac{1}{2\rho D}(b^2 D)_{,k} = 0, \quad \text{(A9)}$$

and hence

$$\int j d\Omega + \frac{h}{u^t} + \int \frac{d(b^2 D)}{2\rho u^t D} = C \quad \text{(A10)}$$

or

$$\int u^t u_\varphi d\Omega + \ln\left(\frac{h}{u^t}\right) + \int \frac{d(b^2 D)}{2\rho h u^t D} = C', \quad \text{(A11)}$$

where $j = h u_\varphi$, C, and C' are constants, and we used the relation derived from the first law of thermodynamics for the isentropic fluid:

$$\frac{P_{,k}}{\rho} = h_{,k}. \quad \text{(A12)}$$

Thus, in the absence of the magnetic fields, Eq. (A10) agrees with Eq. (8). On the other hand, Eq. (A11) with $b^2 = 0$ has been often used for computing differentially rotating neutron stars (e.g., [37,38]).

Equation (A10) or (A11) is used for computing an equilibrium of the torus of toroidal magnetic fields for the case that magnetic fields are confined only in the torus. The magnetic field profile may be arbitrarily given. A simple choice for Eq. (A10) is

$$b^2 D = C_b(\rho u^t D)^n, \quad \text{(A13)}$$

where C_b and $n(>1)$ are constants. Then, the third term of Eq. (A10) is integrated to be

$$\int j d\Omega + \frac{h}{u^t} + \frac{n C_b}{2(n-1)}(\rho u^t D)^{n-1} = C. \quad \text{(A14)}$$

APPENDIX B: CHECKING CONVERGENCE

In the second-order finite-differencing scheme used in this work, the numerical solution for a variable Q at a given

grid point should behave for varying the grid resolution as

$$Q = Q^{(0)} + Q^{(2)}\Delta x^2 + O(\Delta x^3), \tag{B1}$$

where $Q^{(0)}$ and $Q^{(2)}$ are constants and Δx is a local grid spacing. We denote numerical results for three grid resolutions with $\Delta x = \Delta, 2\Delta$, and 4Δ by Q_1, Q_2, and Q_4. Here, Δ is an appropriately chosen grid spacing by which a sufficiently convergent numerical result is obtained. Then, the following relation should hold:

$$R_{\rm con} \equiv \frac{Q_4 - Q_1}{Q_2 - Q_1} = 5. \tag{B2}$$

We refer to $R_{\rm con}$ as the degree of convergence. If the convergence is slower (faster) than that of the second order, the value of $R_{\rm con}$ is smaller (larger) than 5.

To check that Eq. (B2) holds, we performed simulations for a special setting. Here, we present a result for $a = 0.9m$, $r_1 = 1.528\,74m$, $r_2 = 20.3843m$, and $M_* = 0.413\,84m$ with $(N_r, N_\theta) = (800, 100)$, (400, 100), and (200, 100). For the finest grid resolution, we adopted the typical grid setting with $f = 1.01$ and $\Delta r = r_s/50$. For the other two cases, the grid points were chosen as r_{2i} ($i =$ 1–400) and r_{4i} ($i =$ 1–200), respectively, where r_i ($i =$ 1–800) denotes the grid points chosen in the finest grid resolution. For all the grid settings, the grid points are in common located at $r = r_{4i}$, and thus, we compare numerical results there.

In Fig. 11, we show $R_{\rm con}$ at r_{4i} for ϕ, B, q, and $\beta_{\rm T}$ in the equatorial plane as a function of r. It is found that for ϕ, B, and $\beta_{\rm T}$, $R_{\rm con} \approx 5$, showing that the second-order convergence is approximately achieved. Near the horizon, $R_{\rm con}$ is not equal to 5 for $\beta_{\rm T}$. The reason is that we impose the higher-order boundary condition at the horizon for it. For q, $R_{\rm con} =$ 1.5–3, which is much smaller than 5. This is probably because of the fact that the numerical solution is contaminated by an error resulting from the approximate boundary condition. We note that Eq. (47) has an unphysical homogeneous solution, $q \propto \ln r$. We have to exclude the contribution of such a term from the numerical solution, but with the approximate boundary condition used in this work, the exclusion is insufficiently achieved. Nevertheless, the numerical solution gradually converges. This indicates that the contamination by the unphysical solution is not severe. We also note that the global quantities such as mass converge approximately at second order, indicating that the error of q does not play a significant role.

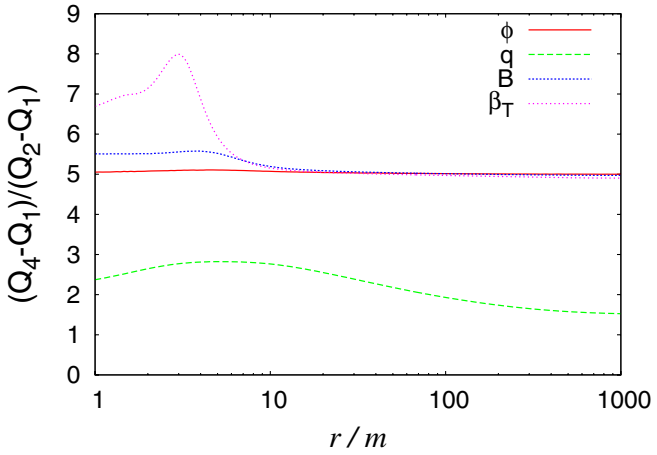

FIG. 11 (color online). Degree of convergence, $R_{\rm con}$, for ϕ, B, q, and $\beta_{\rm T}$ in the equatorial plane.

We performed test simulations for different values of M_* and the results are essentially the same. Convergence of numerical solutions for different grid angular resolutions (but with an identical radial grid) was also performed in the same manner as mentioned above. We adopted $N_\theta = 100$, 50, and 25 and found that the second-order convergence is approximately achieved for ϕ, B, and $\beta_{\rm T}$. Convergence for q is not at second order again, probably because of the same reason as that mentioned above.

APPENDIX C: NEWTONIAN LIMIT OF EQ. (91)

In Appendix B, we consider the Newtonian limit of Eq. (91). Using the standard post-Newtonian prescription (e.g., [39]), $M_{\rm T}$ in the Newtonian limit is written in the form

$$M_{\rm T} = 4\pi \int_{r_s}^{\infty} r^2 dr \int_0^{\pi/2} \sin\theta d\theta \times \rho_* \left(1 + \varepsilon + \frac{3P}{\rho_*} + \Phi_{\rm N} + \frac{3v^2}{2}\right), \tag{C1}$$

where $\Phi_{\rm N}$ is the Newtonian potential and v^2 is the square of the velocity. In the Newtonian case, $\Phi_{\rm N}$ is split into the contribution from the black hole and torus as

$$\Phi_{\rm N} = \Phi_{\rm BH} + \Phi_{\rm t}, \tag{C2}$$

where $\Phi_{\rm BH} = -m/r$ in the Newtonian limit. The gravitational potential energy due to the self-gravity of the torus is

$$W_{\rm t} = \frac{1}{2}\int dV \rho_* \Phi_{\rm t} (<0), \tag{C3}$$

while the gravitational potential energy of the torus due to the gravity of the black hole is

$$W_{\rm BH-t} = \frac{1}{2}\int dV \rho_* \Phi_{\rm BH} (<0). \tag{C4}$$

In the Newtonian limit, rotational kinetic energy T, internal energy U, and volume integral of P, Π are

$$T \equiv \frac{1}{2}\int dV \rho_* v^2, \tag{C5}$$

$$U \equiv \int dV \rho_* \varepsilon, \tag{C6}$$

$$\Pi \equiv \int dVP. \tag{C7}$$

Then, $M_{\rm T}$ is rewritten

$$\begin{aligned} M_{\rm T} &= M_* + U + 2W_{\rm t} + 2W_{\rm BH-t} + 3T + 3\Pi \\ &= (M_* + U + W_{\rm t} + W_{\rm BH-t} + T) \\ &\quad + (3\Pi + W_{\rm t} + 2W_{\rm BH-t} + 2T) - W_{\rm BH-t}. \end{aligned} \tag{C8}$$

Here, $M_* + U + W_{\rm t} + W_{\rm BH-t} + T$ denotes the total energy of the torus (including the rest-mass energy and half of the binding energy between the black hole and torus), and $3\Pi + W_{\rm t} + 2W_{\rm BH-t} + 2T = 0$ because of the virial relation for the equilibrium system [36] (note the factor 2 for the term of $W_{\rm BH-t}$). Thus,

$$M = M_{\rm H} + E_{\rm t} - W_{\rm BH-t}, \tag{C9}$$

where $E_{\rm t}$ denotes the total energy of the torus. Equation (C9) implies that the total energy of the black hole should be $M_{\rm H} - W_{\rm BH-t} > M_{\rm H}$ and the bare mass of the black hole should be larger than $M_{\rm H}$ by a factor of $|W_{\rm BH-t}|$. In other words, $M_{\rm H}$ is smaller than the black hole mass by a factor of the binding energy which is of order $mM_*/r_{\rm t}$ where $r_{\rm t}$ denotes the characteristic radius of the torus. Indeed, the numerical results agree qualitatively with this interpretation.

[1] S. E. Woosley, Astrophys. J. **405**, 273 (1993); B. Paczynski, Astrophys. J. Lett. **494**, L45 (1998).
[2] W. H. Lee and W. Kluzniak, Astrophys. J. **526**, 178 (1999); H. T. Janka, T. Eberl, M. Ruffert, and C. L. Fryer, Astrophys. J. **527**, L39 (1999).
[3] J. A. Faber, T. W. Baumgarte, S. L. Shapiro, and K. Taniguchi, Astrophys. J. **641**, L93 (2006); J. A. Faber, T. W. Baumgarte, S. L. Shapiro, K. Taniguchi, and F. A. Rasio, Phys. Rev. D **73**, 024012 (2006).
[4] M. Shibata and K. Uryū, Phys. Rev. D **74**, 121503(R) (2006); Classical Quantum Gravity **24**, S125 (2007).
[5] M. Shibata and S. L. Shapiro, Astrophys. J. Lett. **572**, L39 (2002).
[6] S. Setiawan, M. Ruffert, and H.-Th. Janka, Mon. Not. R. Astron. Soc. **352**, 753 (2004); W. H. Lee, E. R. Ruiz, and D. Page, Astrophys. J. **632**, 421 (2005).
[7] E.g., J. E. Tohline and I. Hachisu, Astrophys. J. **361**, 394 (1990).
[8] E.g., J. A. Font and F. Daigne, Astrophys. J. **581**, L23 (2002); L. Rezzolla, S. Yoshida, and O. Zanotti, Mon. Not. R. Astron. Soc. **344**, 978 (2003); F. Daigne and J. A. Font, Mon. Not. R. Astron. Soc. **349**, 841 (2004).
[9] M. Shibata, K. Taniguchi, and K. Uryū, Phys. Rev. D **68**, 084020 (2003); **71**, 084021 (2005); M. Shibata and K. Taniguchi, *ibid.* **73**, 064027 (2006).
[10] M. Miller, P. Gressman, and W.-M. Suen, Phys. Rev. D **69**, 064026 (2004).
[11] C. D. Ott, H. Dimmelmeier, A. Marek, H.-T. Janka, I. Hawke, B. Zink, E. Schnetter, Phys. Rev. Lett. **98**, 261101 (2007).
[12] B. Zink *et al.*, Phys. Rev. Lett. **96**, 161101 (2006).
[13] M. D. Duez, Y. T. Liu, S. L. Shapiro, M. Shibata, and B. C. Stephens, Phys. Rev. Lett. **96**, 031101 (2006); M. Shibata, M. D. Duez, Y. T. Liu, S. L. Shapiro, and B. C. Stephens, Phys. Rev. Lett. **96**, 031102 (2006); M. D. Duez, Y. T. Liu, S. L. Shapiro, M. Shibata, and B. C. Stephens, Phys. Rev. D **73**, 104015 (2006); M. Shibata, Y. T. Liu, S. L. Shapiro, and B. C. Stephens, Phys. Rev. D **74**, 104026 (2006).
[14] M. Campanelli, C. O. Lousto, P. Marronetti, and Y. Zlochower, Phys. Rev. Lett. **96**, 111101 (2006); J. G. Baker, J. Centrella, D.-I. Choi, M. Koppitz, and J. van Meter, Phys. Rev. Lett. **96**, 111102 (2006); F. Herrmann, D. Shoemaker, and P. Laguna, arXiv:gr-qc/0601026; B. Brügmann, J. A. Conzalez, M. Hannam, S. Husa, and U. Sperhake, arXiv:gr-qc/0610128.
[15] S. Brandt and B. Brügmann, Phys. Rev. Lett. **78**, 3606 (1997).
[16] B. Brügmann, W. Tichy, and Nina Jansen, Phys. Rev. Lett. **92**, 211101 (2004).
[17] F. Pretorius, Phys. Rev. Lett. **95**, 121101 (2005); A. Buonanno, G. B. Cook, and F. Pretorius, Phys. Rev. D **75**, 124018 (2007).
[18] M. A. Scheel *et al.*, Phys. Rev. D **74**, 104006 (2006).
[19] B. Szilagy *et al.*, Classical Quantum Gravity **24**, S275 (2007).
[20] S. Nishida and Y. Eriguchi, Astrophys. J. **427**, 429 (1994); **461**, 320 (1996).
[21] M. Ansorg and D. Petroff, Phys. Rev. D **72**, 024019 (2005).
[22] D. R. Brill, Ann. Phys. (N.Y.) **7**, 466 (1959).
[23] S. R. Brandt and E. Seidel, Phys. Rev. D **52**, 856 (1995); **52**, 870 (1995).
[24] J. M. Bardeen, in *Black Holes*, editted by C. Dewitt and B. S. Dewitt (Gordon and Breach, New York, 1973), p. 242.
[25] W. Krivan and R. H. Price, Phys. Rev. D **58**, 104003 (1998).
[26] S. Bonazzola and E. Gourgoulhon, Classical Quantum Gravity **11**, 1775 (1994).
[27] S. W. Hawking and G. F. R. Ellis, *The Large Scale Structure of Space-time* (Cambridge University Press, Cambridge, England, 1973).
[28] J. M. Bardeen, B. Carter, and S. W. Hawking, Commun. Math. Phys. **31**, 161 (1973); B. Carter, in *Black Holes*, edited by C. Dewitt and B. S. Dewitt (Gordon and Breach, New York, 1973), p. 57.
[29] L. Smarr, Phys. Rev. Lett. **30**, 71 (1973).
[30] M. Ansorg and D. Petroff, Classical Quantum Gravity **23**, L81 (2006).
[31] D. Christodoulou, Phys. Rev. Lett. **25**, 1596 (1970).

[32] R. Arnowitt, Deser, and C. W. Misner, in *Gravitation: An Introduction to Current Research*, edited by L. Witten (Wiley, New York, 1962), p. 227.
[33] R. Beig, Phys. Lett. A **69**, 153 (1978).
[34] M. Shibata and M. Sasaki, Phys. Rev. D **58**, 104011 (1998).
[35] S. Bonazzola, E. Gourgoulhon, M. Salgado, and J. A. Marck, Astron. Astrophys. **278**, 421 (1993); M. Salgado, S. Bonazzola, E. Gourgoulhon, and P. Haensel, Astron. Astrophys. **291**, 155 (1994).
[36] See, e.g., S. L. Shapiro and S. A. Teukolsky, *Black Holes, White Dwarfs, and Neutron Stars* (Wiley, New York, 1983), Chap. 7.
[37] T. W. Baumgarte, S. L. Shapiro, and M. Shibata, Astrophys. J. Lett. **528**, L29 (2000).
[38] M. Shibata, T. W. Baumgarte, and S. L. Shapiro, Astrophys. J. **542**, 453 (2000).
[39] L. Blanchet, T. Damour, and G. Schäfer, Mon. Not. R. Astron. Soc. **242**, 289 (1990); H. Asada, M. Shibata, and T. Futamase, Prog. Theor. Phys. **96**, 81 (1996).